AAS 23-152

TERMINAL LANDING GUIDANCE LAW USING ANALYTIC GRAVITY TURN TRAJECTORY

Seungyeop Han [*], **Koki Ho** [†]

This paper introduces the terminal landing guidance law based on the analytic solution of gravity-turn trajectory. Characteristics of the derived solution are investigated, and the solution is used for the generation of a reference two-dimensional vector field that satisfies terminal landing conditions. In addition, the vector field is further expanded to consider ground collision avoidance as well as three-dimensional problem. A nonlinear control law is applied to track the reference vector efficiently within a finite time. The effectiveness of the proposed method is demonstrated through nonlinear numerical simulations, and performances are compared with existing methods.

INTRODUCTION

Moon and Mars explorations have intrigued many researchers for a long period of time. From the past to the present, numerous projects related to these explorations have been launched and vigorously studied. Among many projects, the representative projects would be Apollo and Artemis missions for lunar exploration, and Opportunity, Curiosity, and Perseverance missions are well-known projects for Mars exploration.[1,2] The aforementioned projects have to safely land their sophisticated lander or rover to conduct exploration missions. Therefore, many works on the powered descent and final soft landing method of the lander using a thruster have been studied. Furthermore, there are a number of studies on the landing method of lifting bodies using a thruster while taking advantage of its lifting body.[3,4] In order to achieve a safe landing at the desired landing site, it is important to design proper terminal landing guidance law.

Most works can fall into two groups: 1) computational guidance and 2) classical feedback guidance. Methods in the former group reconstruct the landing problem as an optimization problem and solve the problem numerically. One representative approach is the fuel optimal problem through convex programming with aid of lossless convexification on thrust constraint.[5] The extended work has demonstrated that a fuel optimal trajectory can be obtained within a short period of time under limited onboard computation power.[6] Yet another famous approach for solving the fuel optimal problem is using the optimal control theory.[7] This method converts the landing problem into a multivariable root-finding problem via optimality conditions, which enables solving the problem quickly.

There are many different approaches to feedback type guidance methods. The three most well-developed approaches include polynomial guidance used for the Apollo program, gravity turn guidance for the Surveyor and Phoenix program, and zero-effort-miss & zero-effort-velocity (ZEM/ZEV)

[*]PhD Student, Daniel Guggenheim School of Aerospace Engineering, Georgia Institute of Technology, Atlanta, GA,30332
[†]Associate Professor, Daniel Guggenheim School of Aerospace Engineering, Georgia Institute of Technology, Atlanta,GA, 30332

guidance.[8–11] Among many variants of polynomial guidance, the guidance law using a third-order polynomial for each axis control has been introduced.[12] The method can effectively handle a pin-point landing for the preferred initial condition, but the effectiveness of the method is not verified for general cases. Many works using ZEM/ZEV have been done to make the original ZEM/ZEV law suitable for the landing problem. Multiple waypoints ZEM/ZEV method shows the fuel-efficient trajectory while satisfying state constrain.[13] Another modification introduced a constant-thrust phase in addition to the ZEM/ZEV guidance law to shape the curvature of trajectory.[14] The guidance law using a gravity turn trajectory has been published to handle the soft landing of two-Dimensional planar motion.[9,15] The extended work adopted a nonlinear control theory to make the logic more effective.[16] Another extended study developed the concept to explain the logic of three-dimensional motion.[17]

The logic of this paper can be classified as feedback guidance using the solution of gravity turn trajectory. The trajectory is beneficial to meet obstacle avoidance constraints as well as secure the sensor field of view availability due to its concave down shape. In addition, the direction of the thrust vector will be aligned with the local gravitational direction at the last moment. Therefore, it ensures the correct attitude of the vehicle meaning that the lander stands upright after landing. The proposed law also guarantees the finite time error convergence with robustness against disturbances. Unlike most previous works, it is closed-form and does not require any online optimization, so it is suitable for practical systems with limited computational power.

The rest of the paper is organized as follows. First, the paper reviews the analytic solution of gravity turn trajectory and explains how to compute the desired descent velocity vector based on the solution. Based on the results made previously, the paper presents the velocity vector tracking control law that guarantees finite time convergence and has robustness against disturbance. Then, the effectiveness of the proposed method is demonstrated through 3-Dimensional nonlinear numerical simulations under various three representative scenarios cases, and performances are compared with existing non-iterative methods.

ANALYTIC SOLUTION OF GRAVITY TURN TRAJECTORY

The terminal phase, which is the last phase of EDL, shows different dynamic characteristics compared to other landing phases. During the terminal landing phase, the altitude, as well as the velocity of the lander, are relatively low. Therefore, some reasonable approximation can be applied to derive the analytic solution. The goals of this section are to obtain the analytic solution for the approximated gravity turn trajectory and to investigate the useful properties for guidance law design.

Equation of motion for the lander

Referring to Figure 1, the local reference frame L with basis vector $\{\hat{x}_L, \hat{y}_L, \hat{z}_L\}$ is fixed with respect to the ground surface, and the landing site is set to be the origin of the frame without loss of generality. For the terminal phase case, the non-inertial frame can be ignored and the gravitational acceleration can be reasonably considered as a constant, respectively. Then, the three-dimensional point-mass equations describing the motion of the lander can be written as follows,

$$m\dot{\vec{v}} = \vec{T} + m\vec{g} + \vec{d} \tag{1a}$$

$$\dot{\vec{r}} = \vec{v} \tag{1b}$$

$$\dot{m} = -\alpha \|\vec{T}\| \tag{1c}$$

where $\vec{v}$ is the velocity vector of the lander, $\vec{r}$ is the position velocity vector of the lander, $\vec{T}$ is the net thrust vector, $\vec{g}$ is the local gravitational acceleration vector, $\vec{d}$ is the total disturbance vector, m is the lander mass, and α is a positive constant describing the fuel consumption rate.

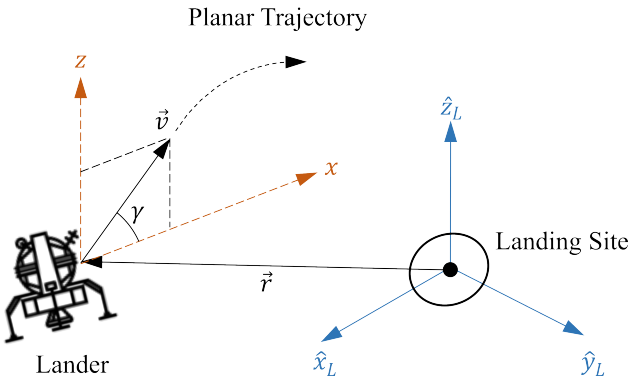

Figure 1. Terminal Phase Landing Geometry and Planar Motion

Analytic Solution of Powered Descent Gravity Turn Trajectory

The gravity turn trajectory is the trajectory where the gravitational force is a major force that changes the flight-path angle, and this can be achieved simply by aligning $\vec{T}$ to $\vec{v}$. In this case, the motion becomes two-dimensional planar motion as in Figure 1. It is well-known that the optimal thrust profile minimizing fuel consumption is bang-off-bang control, and the profile has at most two switches between the min-max control bounds.[7] Therefore, applying near-maximum deceleration would require less fuel usage while giving additional margin to correct guidance errors and overcome unknown disturbances. If the lander applies constant thrust acceleration and the disturbances are ignored, then the equations for planar motions become

$$\frac{dv}{dt} = -\beta g - g \sin\gamma \tag{2a}$$

$$v\frac{d\gamma}{dt} = -g \cos\gamma \tag{2b}$$

$$\frac{dx}{dt} = v \cos\gamma \tag{2c}$$

$$\frac{dz}{dt} = v \sin\gamma \tag{2d}$$

where $\beta \equiv T/mg$ is the constant normalized acceleration (thrust to weight ratio) due to the near-maximum thrust, g is the norm of $\vec{g}$, γ is the flight-path angle, x is the downrange and z is the height of the lander along the planar motion.

Note that the γ and t show the monotonic relation, so the change of the independent variable of t to γ can be done by dividing Eqs. (2a), (2c), and, (2d) by Eq. (2b) as follows[18]

$$\frac{dv}{d\gamma} = v\tan\gamma + \beta\sec\gamma \tag{3a}$$

$$\frac{dt}{d\gamma} = -\frac{v}{g}\sec\gamma \tag{3b}$$

$$\frac{dx}{d\gamma} = -\frac{v^2}{g} \tag{3c}$$

$$\frac{dz}{d\gamma} = -\frac{v^2}{g}\tan\gamma \tag{3d}$$

The analytic solution of Eq. (3) is known as follows.[18]

$$v(\gamma) = C\sec\gamma\left(\sec\gamma + \tan\gamma\right)^{\beta} \tag{4a}$$

$$t(\gamma) = t(\gamma_0) - \frac{C}{g}\left[F_t(\gamma) - F_t(\gamma_0)\right] \tag{4b}$$

$$x(\gamma) = x(\gamma_0) - \frac{C^2}{g}\left[F_x(\gamma) - F_x(\gamma_0)\right] \tag{4c}$$

$$z(\gamma) = z(\gamma_0) - \frac{C^2}{g}\left[F_z(\gamma) - F_z(\gamma_0)\right] \tag{4d}$$

where γ_0 is the initial flight path angle, C is the integration constant defined as

$$C = \frac{v(\gamma_0)}{\sec\gamma_0\left(\sec\gamma_0 + \tan\gamma_0\right)^{\beta}} \tag{5}$$

F_t, F_x and F_z are the indefinite integral as

$$F_t(\gamma) = \frac{1}{\beta^2 - 1}(\beta\sec\gamma - \tan\gamma)(\sec\gamma + \tan\gamma)^{\beta} \tag{6a}$$

$$F_x(\gamma) = \frac{1}{4\beta^2 - 1}(2\beta\sec\gamma - \tan\gamma)(\sec\gamma + \tan\gamma)^{2\beta} \tag{6b}$$

$$F_z(\gamma) = \frac{1}{4\beta^2 - 4}(2\beta\sec\gamma\tan\gamma - 2\tan^2\gamma - 1)(\sec\gamma + \tan\gamma)^{2\beta} \tag{6c}$$

Characteristics of Powered Descent Gravity-Turn Trajectory

[19] Before applying the solution for guidance law design, it is important to understand the properties of the solution trajectory. Without loss of generality, a flight path angle is assumed to be $\gamma \in [-\frac{\pi}{2}, \frac{\pi}{2}]$ only for analysis purposes.

Characteristic 1: Along the trajectory, the flight-path angle γ converges to $-\pi/2$ so the thrust direction becomes parallel to the nadir.

Proof: Let $\Gamma \equiv \gamma + \pi/2$, then $\Gamma^2 > 0$ for $\Gamma \neq 0$ and $\Gamma^2 = 0$ for $\Gamma = 0$. The time derivative of Γ^2 along the trajectory is

$$\frac{d}{dt}\Gamma^2 = -2\frac{g}{v}\Gamma \sin\Gamma\dot{\gamma} \tag{7}$$

from Eq. (2b) meaning that $\dot{\Gamma^2} < 0$ for $\Gamma \in (0, \pi)$. By the Lyaponov stability theorem, $\Gamma \to 0$ or equivalently $\gamma \to -\pi/2$ as $t \to \infty$. Therefore, an upper limit value of γ for the solutions Eq. (4) is $-\pi/2$, and both velocity and thrust direction become parallel to the nadir as descend.

Characteristic 2: Along the trajectory with $\beta > 1$, $v \to 0$ as $\gamma \to -\pi/2+$ within finite time. Consequently, downrange as well as altitude variation are finite.

Proof: For $a \geq 0, b > 0$, following identity holds

$$\sec^a\gamma(\sec\gamma + \tan\gamma)^b = \frac{(1+\sin\gamma)^b(1-\sin\gamma)^b}{\cos^{a+b}\gamma(1-\sin\gamma)^b} = \frac{\cos^{b-a}\gamma}{(1-\sin\gamma)^b} \tag{8}$$

Then limit value of Eq. (8) when $b - a > 0$ is

$$\lim_{\gamma\to-\frac{\pi}{2}+}\frac{\cos^{b-a}\gamma}{(1-\sin\gamma)^b} = 0 \quad \text{for} \quad b-a>0 \tag{9}$$

The Eq. (4a) belongs to the particular case of Eq. (8) with $a = 1$ and $b = \beta > 1$ by assumption, hence $v \to 0$ as $\gamma \to -\pi/2+$. On the other hand, the following trigonometric inequalities hold

$$0 \leq |\tan\gamma| \leq |\sec\gamma|, \quad 0 \leq |\tan^2\gamma| \leq |\sec^2\gamma|, \quad 0 \leq |\sec\gamma\tan\gamma| \leq |\sec^2\gamma| \tag{10}$$

for $\gamma \in (-\frac{\pi}{2}, \frac{\pi}{2})$. One can make the lower and upper bound of Eq. (6) be the particular case of Eq. (8) using Eq. (10). Then, the limit value of Eq. (6) can be obtained by applying the squeeze theorem.

$$\lim_{\gamma\to-\frac{\pi}{2}+}F_t(\gamma) = \lim_{\gamma\to-\frac{\pi}{2}+}F_x(\gamma) = \lim_{\gamma\to-\frac{\pi}{2}+}F_z(\gamma) = 0 \tag{11}$$

These imply that variation of time, downrange, and altitude is finite during the gravity turn phase, if $\beta > 1$. In other words, $v \to 0$, $\gamma \to -\pi/2$ within finite time, and the terminal value of Eq. (6) can be simplified as follow

$$x_f = x_0 + \frac{v_0^2}{(4\beta^2-1)g}(2\beta\cos\gamma_0 - \sin\gamma_0\cos\gamma_0) \tag{12a}$$

$$z_f = z_0 + \frac{v_0^2}{(4\beta^2-4)g}(2\beta\sin\gamma_0 - \sin^2\gamma_0 - 1) \tag{12b}$$

$$t_f = t_0 + \frac{v_0}{(\beta^2 - 1)g}(2\beta - \sin\gamma_0) \tag{12c}$$

where subscript 0 implies the initial states and subscript f means the final states (when $v = 0$), respectively.

TERMINAL LANDING VELOCITY VECTOR FIELD

Referring to Eq. (12a) and Eq. (12b) and treating x_f and z_f as the desired landing location give the two nonlinear equations described by initial states (x_0, z_0, v_0, γ_0) and trajectory parameters (β, g). For fixed values (x_f, z_f, g), the number of equations is only two compared to five variables (x_0, z_0, v_0, γ_0, β), which is an under-determined problem, and the paper choose v and γ as representative parameters. From now on, we will omit the subscription 0 for readability. Then the nonlinear state equations can be re-expressed as follow

$$f_x(v, \gamma, \beta, x_{go}) = (4\beta^2 - 1)x_{go} - \frac{v^2}{g}(2\beta c_\gamma - s_\gamma c_\gamma) \tag{13a}$$

$$f_z(v, \gamma, \beta, z_{go}) = (4\beta^2 - 4)z_{go} - \frac{v^2}{g}(2\beta s_\gamma - s_\gamma^2 - 1) \tag{13b}$$

where $x_{go} \equiv x_f - x$, $z_{go} \equiv z_f - z$, $c_\gamma \equiv \cos\gamma$, and $s_\gamma \equiv \sin\gamma$. Note that there are infinitely many solution sets $\{v, \gamma, \beta, x_{go}, z_{go}\}$ satisfying $f_x = f_z = 0$, but it turns out that v and γ are uniquely determined for specific x_{go}, z_{go}, and $\beta > 1$, and this relationship will map a velocity vector field. In this section, the vector field will be elucidated.

Uniqueness and Existence of Desired Velocity Vector

From Eq. (13a), the proper range of γ can be determined by sign of x_{go}, and the paper assumes $x_{go} \geq 0$ or equivalently $\gamma \in [-\frac{\pi}{2}, \frac{\pi}{2}]$ only for simplification of derivation.

Case 1: $x_{go} \neq 0$

Rearranging $f_x(v, \gamma) = f_z(v, \gamma) = 0$ defines single-variable function $h(\gamma)$ with $\kappa \equiv \frac{(4\beta^2-4)z_{go}}{(4\beta^2-1)x_{go}}$

$$h(\gamma) \equiv \frac{2\beta s_\gamma - s_\gamma^2 - 1}{2\beta c_\gamma - s_\gamma c_\gamma} - \kappa \tag{14}$$

By the assumption κ is bounded, and $h(\gamma) \to \infty$ as $\gamma \to \frac{\pi}{2}^-$ and $h(\gamma) \to -\infty$ as $\gamma \to -\frac{\pi}{2}^+$. Derivative of $h(\gamma)$ with respect to γ is

$$\frac{dh}{d\gamma} = \frac{3(\beta - s_\gamma)^2 + \beta^2 - 1}{(2\beta c_\gamma - s_\gamma c_\gamma)^2} \tag{15}$$

and it turns out to be strictly positive. The intermediate value theorem with strict monotonicity of $h(\gamma)$ guarantees the unique solution γ^* that makes $h(\gamma^*) = 0$. Due to the monotonicity of $h(\gamma)$, any single-variable numerical root-finding method can obtain an accurate solution within a few iterations. Note that the following equation gives a good enough initial guess.

$$\gamma^{(0)} = \tan^{-1}\left(\frac{z_{go}}{x_{go}}\right) \tag{16}$$

Once γ^* is determined, then v^* can be computed by original equation as follows

$$v^* = \sqrt{\frac{(4\beta^2 - 1)gx_{go}}{(2\beta - s_{\gamma^*})c_{\gamma^*}}} \tag{17}$$

Case 2: $x_{go} = 0$
The condition $x_{go} = 0$ means $c_{\gamma^*} = 0$, which implies that either $\gamma^* = \frac{\pi}{2}$ or $\gamma^* = -\frac{\pi}{2}$. The correct solutions are obtained as follows, which are identical to that of one-dimensional constant acceleration motion.

$$(v^*, \gamma^*) = \begin{cases} \left(\sqrt{2(\beta+1)gz_{go}}, \frac{\pi}{2}\right), & \text{if } z_{go} \geq 0 \\ \left(\sqrt{-2(\beta-1)gz_{go}}, -\frac{\pi}{2}\right), & \text{if } z_{go} < 0 \end{cases} \tag{18}$$

Once v^* and γ^* are obtained, $v_x^* = v^* \cos\gamma^*$ and $v_z^* = v^* \sin\gamma^*$ are computed for later control usage. Like the case of subscription 0, $*$ notation will be omitted if it is clear from the context.

Properties of Velocity Vector Field

In this subsection, we will investigate the overall properties of the velocity vector field derived in the previous subsection.

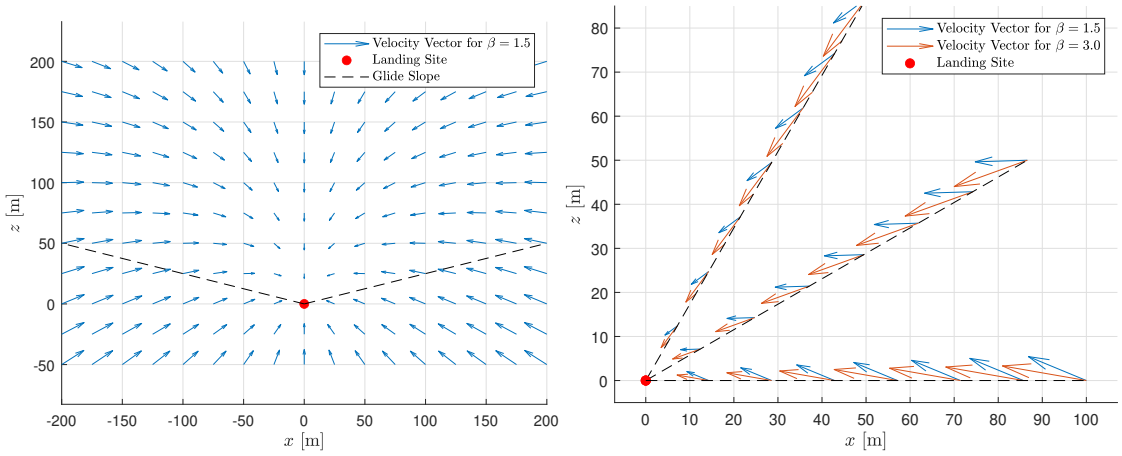

Figure 2. (a) Velocity Vector Field and (b) Positional and Acceleration Sensitivity

Characteristic 1: The trajectory of a vehicle along the vector field is concave down about the landing position, meaning that the vehicle always flies over the line of sight(LOS) vector as shown in Figure 2. This property is appropriate for the lander since it helps avoid hazardous obstacles around the landing area and secure the visibility of camera field of view.[14]

Proof: Comparing z_{go}/x_{go} and s_γ/c_γ gives

$$\begin{aligned} \frac{s_\gamma}{c_\gamma} - \frac{z_{go}}{x_{go}} &= \frac{s_\gamma\left(4\beta^2 - 4\right)\left(2\beta c_\gamma - s_\gamma c_\gamma\right) - c_\gamma\left(4\beta^2 - 1\right)\left(2\beta s_\gamma - s_\gamma^2 - 1\right)}{c_\gamma\left(4\beta^2 - 4\right)\left(2\beta c_\gamma - s_\gamma c_\gamma\right)} \\ &= \frac{4\beta^2 + 3(\beta - s_\gamma)^2}{\left(4\beta^2 - 4\right)\left(2\beta c_\gamma - s_\gamma c_\gamma\right)} > 0 \end{aligned} \tag{19}$$

proving that γ is always larger than LOS angle as long as the vehicle is on the trajectory as illustrated in Figure 2.

Characteristic 2: For constant β, the velocity vector along the LOS vector from the landing site to the vehicle has identical vector direction (γ^*). Additionally, moving outward along the LOS vector from the origin increase the magnitude of vector (v^*), and the statements are illustrated in Figure 2.

Proof: If remaining height to downrange ratio z_{go}/x_{go} is maintained by assumption, then so as the κ introduced at Eq. (14). Therefore, original γ^* will satisfy the $h(\gamma^*) = 0$ regardless of z_{go} and x_{go} variation as long as z_{go}/x_{go} is constant. In addition, Eqs (13a) can be rearranged as $x_{go} = c_1 v^2$ for constant scalar value c_1 because γ^* becomes constant by assumption. Therefore, increasing or decreasing the range from the landing site to the vehicle will increase or decrease the magnitude of the vector field.

Characteristic 3: For fixed x_{go} and z_{go}, variation of β changes v as well as γ of vector-field. Although detail procedures are omitted, it turns out that larger β makes v larger while γ smaller and vice versa for fixed x_{go} and z_{go}. In other words, the velocity vector field of small β makes a steep and slow landing trajectory as shown in Figure 2.

On the other hand, following the maximum acceleration $(\beta) = C_\beta \beta_{\max}$ trajectory uses less fuel for landing but there are always initial handover errors from the previous guidance phase and multiple disturbances. Therefore, selecting appropriate C_β is necessary through environment modeling, system budgeting, and iterative simulations, and the ratio 0.9 is used for the paper.

Characteristic 4: Let assume that the lander precisely follows the vector field of acceleration β, then the remaining time until landing is

$$t_{go}(\beta) = \frac{v}{(\beta^2 - 1)g}(\beta - s_\gamma) \tag{20}$$

and the result is used for time-to-go estimation of the guidance law which will be explained in the subsequent section. Additionally, due to the constant acceleration level along the trajectory, overall acceleration usage during landing is βt_{go}. This could be applied for a feasibility check of the current landing site, but this is beyond the scope of the paper.

TERMINAL LANDING GUIDANCE LAW

Velocity Tracking Control Law

Referring to Figure 3, the guidance reference frame G with basis vectors $\{\hat{x}_G, \hat{y}_G, \hat{z}_G\}$ is additionally introduced and it is defined through a rotation of the frame L with angle θ along $\hat{z}_L$ axis. The value of θ is computed as

$$\theta = \text{atan2}\left(-r_{y_L}, -r_{x_L}\right) \tag{21}$$

where r_{x_L}, r_{y_L}, and r_{z_L} are vector elements of $\vec{r}^L = \begin{bmatrix} r_{x_L} & r_{y_L} & r_{z_L} \end{bmatrix}^\top$ which is the vector $\vec{r}$ expressed in the frame R. Then the frame transformation matrix from the L frame to the G frame is simply

$$T_{G/L} = \begin{bmatrix} \cos\theta & \sin\theta & 0 \\ -\sin\theta & \cos\theta & 0 \\ 0 & 0 & 1 \end{bmatrix} \tag{22}$$

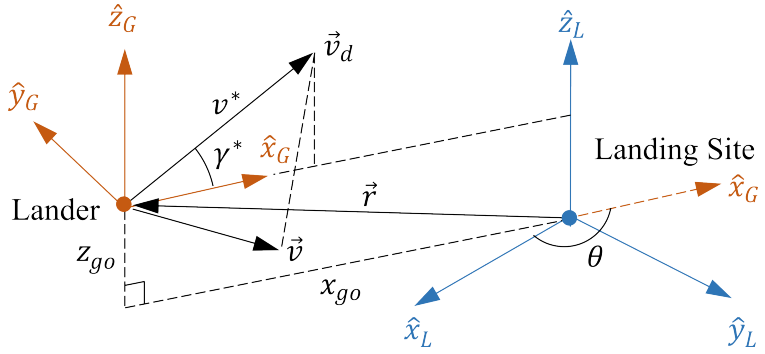

Figure 3. Illustration Caption Goes Here

In order to make the lander fly toward the landing site, the desired velocity vector of the lander $\vec{v}_d$ always resides on the $\hat{x}_G - \hat{z}_G$ plane, and the magnitude v^* and the direction γ^* of the vector are computed using the value x_{go} and z_{go}.

$$\vec{v}_d^{\,G} = \begin{bmatrix} v^* \cos\gamma^* \\ 0 \\ v^* \sin\gamma^* \end{bmatrix} = \begin{bmatrix} v_x^* \\ 0 \\ v_z^* \end{bmatrix} \tag{23}$$

Let $\vec{e} \equiv \vec{v}_d - \vec{v}$ be the velocity tracking error vector. Then the time derivative of $\vec{e}$ with respect to frame L is computed as

$$\begin{aligned} {}^L\dot{\vec{e}} &= {}^L\dot{\vec{v}}_d - {}^L\dot{\vec{v}} \\ &= {}^G\dot{\vec{v}}_d + \vec{\omega}_{G/L} \times \vec{v}_d - (\vec{u} + \vec{g} + \vec{d}) \end{aligned} \tag{24}$$

where $\vec{\omega}_{G/L}$ is the angular velocity vector of the frame G with respect to the frame L, and the left superscript on the vector derivative indicates the frame where the derivative is computed.

Next, the way to compute the term ${}^G\dot{\vec{v}}_d$ and $\vec{\omega}_{G/L}$ will be investigated. By the chain rule of differentiation, the term ${}^G\dot{\vec{v}}_d$ expressed in frame G is equal to

$${}^G\dot{\vec{v}}_d^{\,G} = F_{v_d} F_{r_{go}} \vec{v}^G \tag{25}$$

where

$$F_{v_d} = \frac{1}{\frac{\partial f_x}{\partial v_x^*}\frac{\partial f_z}{\partial v_z^*} - \frac{\partial f_z}{\partial v_x^*}\frac{\partial f_x}{\partial v_z^*}} \begin{bmatrix} \frac{\partial f_z}{\partial v_z^*} & 0 & -\frac{\partial f_x}{\partial v_z^*} \\ 0 & 0 & 0 \\ -\frac{\partial f_z}{\partial v_x^*} & 0 & \frac{\partial f_x}{\partial v_x^*} \end{bmatrix} \tag{26a}$$

$$\frac{\partial f_x}{\partial v_x^*} = \frac{1}{v^*}\left(2\beta(v_x^*)^2 + 2\beta(v^*)^2 - v^* v_z^*\right) \tag{26b}$$

$$\frac{\partial f_x}{\partial v_z^*} = \frac{1}{v^*}\left(2\beta v_x^* v_z^* - v^* v_x^*\right) \tag{26c}$$

$$\frac{\partial f_z}{\partial v_x^*} = \frac{1}{v^*}\left(2\beta v_x^* v_z^* - 2v^* v_x^*\right) \tag{26d}$$

$$\frac{\partial f_z}{\partial v_z^*} = \frac{1}{v^*}\left(2\beta(v_z^*)^2 + 2\beta(v^*)^2 - 4v^* v_z^*\right) \tag{26e}$$

and

$$F_{r_{go}} = \begin{bmatrix} \frac{\partial f_x}{\partial x_{go}} & 0 & \frac{\partial f_x}{\partial z_{go}} \\ 0 & 0 & 0 \\ \frac{\partial f_z}{\partial x_{go}} & 0 & \frac{\partial f_z}{\partial z_{go}} \end{bmatrix} \tag{27a}$$

$$\frac{\partial f_x}{\partial x_{go}} = -(4\beta^2 - 1)g, \quad \frac{\partial f_x}{\partial z_{go}} = 0 \tag{27b}$$

$$\frac{\partial f_z}{\partial z_{go}} = -(4\beta^2 - 4)g, \quad \frac{\partial f_z}{\partial x_{go}} = 0 \tag{27c}$$

For the case of $\vec{\omega}_{G/L}$, the $\hat{y}_G$ velocity component of the lander will make the relative angular velocity as follow (The detailed derivation procedure for computing a generalized angular velocity can be found in Han's work).[20]

$$\vec{\omega}_{G/L}^{L} = \vec{\omega}_{G/L}^{G} = \frac{-(\vec{r}\cdot\hat{x}_G)\hat{x}_G^G \times (\vec{v}^G - (\vec{v}\cdot\hat{z}_G)\hat{z}_G^G)}{(\vec{r}\cdot\hat{x}_G)^2} = \begin{bmatrix} 0 \\ 0 \\ -\frac{v_{y_G}}{x_{go}} \end{bmatrix} \tag{28}$$

The For the case of $\vec{\omega}_{G/L}$, the $\hat{y}_G$ velocity component of the lander will make the relative angular velocity as follow.

With the previously developed results, this paper proposes the velocity tracking guidance law by adopting the structure of the nonlinear control law suggested by Lee.[21]

$$\vec{u} = {}^G\dot{\vec{v}}_d + \vec{\omega}_{G/L} \times \vec{v}_d - \vec{g} + \frac{k}{\hat{t}_{go}}\vec{e} \tag{29}$$

Note that either the frame L or G can be selected for the computation of the Eq. (29), and this paper used the frame G to present the command explicitly.

$$\begin{aligned} \vec{u}^G &= F_{v_d}F_{r_{go}}\vec{v}^G + \vec{\omega}_{G/L}^G \times \vec{v}_d^G - \vec{g}^G + \frac{k}{\hat{t}_{go}}\vec{e}^G \\ &= \left\{-\beta g\frac{\vec{v}_d^G}{v_d}\right\} + \left\{\frac{k}{\hat{t}_{go}}\vec{e}_v^G\right\} + \left\{F_{v_d}F_{r_{go}}\vec{e}^G + \Omega\vec{e}^G\right\} \end{aligned} \tag{30}$$

where $\Omega = \text{diag}(0, v_x^*/x_{go}, 0)$, and the detailed derivation procedures are omitted due to the page limitation. Note that the proposed law consists of three terms distinguished by braces: gravity-turn acceleration, tracking error feedback acceleration, and reference trajectory perturbation compensation acceleration. In addition, the following equation is used for time-to-go estimation.

$$\hat{t}_{go} = \frac{v_d}{(\beta^2 - 1)g}(\beta - \sin\gamma_d) + \frac{||\vec{e}||}{(\beta_{\max} - \beta)g} \tag{31}$$

Characteristics of Velocity Tracking Control Law

Characteristic 1: If $k \geq 0$, the final time is fixed, and the system is free from disturbances, then the error dynamics will be converged within the desired time.

Proof: By assumption the desired time is determined as fixed value t_f, hence time-to-go is $t_{go} = t_f - t$. Substituting the law Eq. (29) to the error dynamics Eq. (24) reveals the following closed-loop dynamics.

$$\dot{\vec{e}} + \frac{k}{t_{go}}\vec{e} = 0 \tag{32}$$

The above differential equation is a typical first-order Cauchy-Euler equation, and the closed-loop solution can be determined as follows

$$\vec{e}(t_{go}) = \left(\frac{t_{go}}{t_f}\right)^k \vec{e}(t_0) \tag{33}$$

where $\vec{e}(t_0)$ is the initial tracking error. Therefore, the system is stable, and tracking error converges to zero as $t_{go} \to 0$ (i.e $t \to t_f$), if $k \geq 0$.

Characteristic 2: If $k > 1$ and the system is free from disturbances, the acceleration command will converge to the gravity-turn acceleration of β as $t_{go} \to 0$.

Proof: Substituting the closed-loop solution of error vector Eq. (33) into the tracking law Eq. (30) results the following.

$$\vec{u}^G = -\beta g \frac{\vec{v}_d^G}{v_d} + k\frac{t_{go}^{k-1}}{t_f^k}\vec{e}^G(t_0) + \left(F_{v_d}F_{r_{go}} + \Omega\right)\left(\frac{t_{go}}{t_f}\right)^k \vec{e}^G(t_0) \tag{34}$$

First of all, the matrix term $\left(F_{v_d}F_{r_{go}} + \Omega\right)$ is bounded for the entire region. Therefore, the acceleration command will gradually converge to final gravity-turn acceleration as $t_{go} \to 0$, if $k > 1$, as desired.

$$\lim_{t_{go}\to 0} \vec{u} = -\beta g \frac{\vec{v}_d}{v_d} \tag{35}$$

Characteristic 3: If $k > 1$ and the magnitude of disturbances is bounded by the constant value d_{max}, then the error will be converged within the desired time.

Proof: If there exist disturbances, then the error dynamic becomes

$$\dot{\vec{e}} + \frac{k}{t_{go}}\vec{e} = \vec{d} \tag{36}$$

One can rewrite the equation for each axis since they are decoupled.

$$\dot{e}_i + \frac{k}{t_{go}}e_i = d_i \quad i = x, y, z \tag{37}$$

The solution of Eq. (39) is

$$e_i(t) = \left(\frac{t_{go}}{t_f}\right)^k e_i(t_0) + t_{go}^k \int \frac{d_i(\tau)}{t_{go}^k(\tau)} d\tau \tag{38}$$

Since the disturbance is bounded, the following inequality holds.

$$
\begin{aligned}
|e_i(t)| &= \left| \left(\frac{t_{go}}{t_f}\right)^k e_i(t_0) + t_{go}^k \int \frac{d_i(\tau)}{t_{go}^k(\tau)} d\tau \right| \\
&\leq \left(\frac{t_{go}}{t_f}\right)^k |e_i(t_0)| + t_{go}^k \int \frac{|d_i(\tau)|}{t_{go}^k(\tau)} d\tau \\
&\leq \left(\frac{t_{go}}{t_f}\right)^k |e_i(t_0)| + \frac{t_{go}}{k-1} d_{max}
\end{aligned}
\tag{39}
$$

The result shows that $e_i(t) \to 0$ as $t_{go} \to 0$ or equivalently $\vec{e} \to 0$ as $t_{go} \to 0$. In addition, the second term of Eq. (34) will no longer converge to zero but will have some value owing to the non-zero disturbances. As a result, the last moment acceleration command will have some bias terms in addition to the pure gravity-turn acceleration.

Ground Collision Avoidance Logic

In practice, there could exist ground obstacles near the landing site so the glide slope constraint should be considered to avoid a collision. The gravity turn trajectory automatically satisfies the constraint thanks to its concave-down shape so the constraint does not need to be considered once the tracking error is sufficiently reduced. However, the lander could collide with an obstacle as reducing the tracking error, so additional collision avoidance logic should be implemented when the tracking error exceeds the user-defined threshold: $\|\vec{e}\| > C_e$.

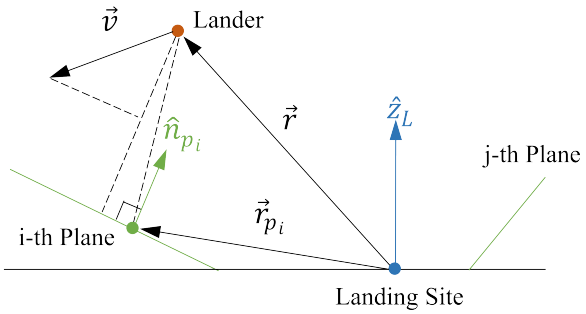

Figure 4. Collision Avoidance Geometry with Obstacle Planes

Referring to Figure. 4, let's assume the obstacles are bounded by multiple planes. Then the required deceleration for a full stop just before the collision with the i-th plane is computed as follows.

$$
\vec{a}_{\text{col}} = \left(-(\vec{g} \cdot \hat{n}_{p_i}) + \frac{(\vec{v} \cdot \hat{n}_{p_i})^2}{2(\vec{r} - \vec{r}_{p_i}) \cdot \hat{n}_{p_i}} \right) \hat{n}_{p_i} \tag{40}
$$

where $\hat{n}_{p_i}$ is the unit normal vector of the i-th plane toward $\hat{z}_L$ direction and $\vec{r}_{p_i}$ is the position vector on the i-th plane.

In order to reduce the unnecessary collision avoidance action, the action will be triggered only when the a_n exceeds the user-defined acceleration threshold; $\|\vec{a}_{\text{col}}\| > C_{\text{col}} \beta_{\max} g$. In order to utilize the logic, the glide slope constraint should be expressed with a plane. Referring to Figure. 5, the

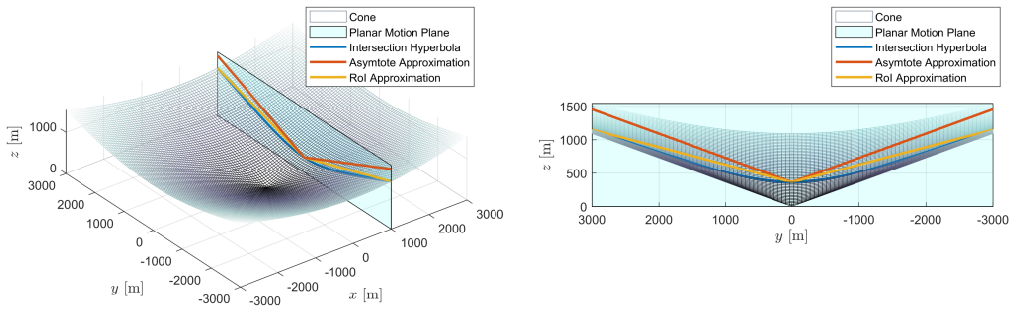

Figure 5. Obstacle Plane Approximation of Glide Slope Cone

instantaneous glide slope constraint can be roughly bounded by an asymptote of a hyperplane or rather tightly by considering the maximum region of interest. Once the slope is approximated, Eq. (40) can be applied.

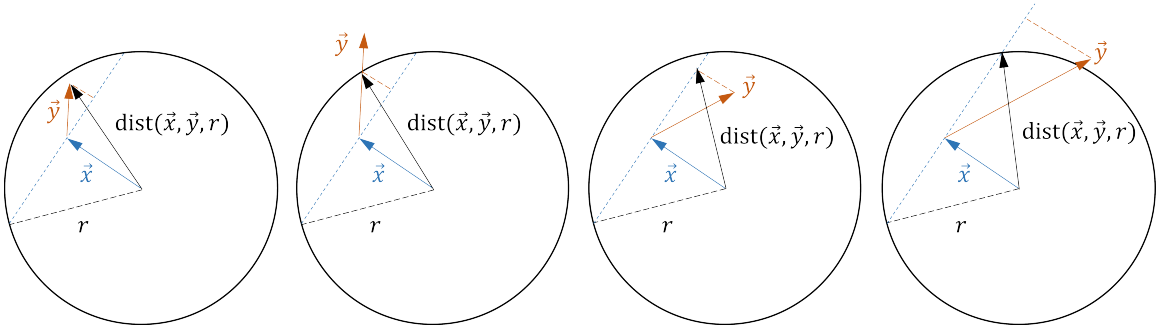

Figure 6. Allocation of Tracking Command and Collision Avoidance Command

Lastly, if the required deceleration exceeds the threshold level, then the acceleration command for collision avoidance $\vec{a}_{\text{col}}$ must be prioritized over the velocity tracking command $\vec{a}_{\text{trk}}$. To incorporate the priority of the command, the following acceleration command is applied if the collision avoidance logic is triggered.

$$\vec{u} = \vec{a}_{\text{col}} + \text{dist}(\vec{a}_{\text{col}}, \vec{a}_{\text{trk}}, \beta_{\max} g) \tag{41}$$

where the vector allocation function dist is defined as following equation and Figure. 6.

$$\text{dist}(\vec{x}, \vec{y}, r) = \begin{cases} \text{sat}\left(\vec{y} - (\vec{y} \cdot \frac{\vec{x}}{\|\vec{x}\|})\frac{\vec{x}}{\|\vec{x}\|}, \sqrt{r^2 - \vec{x} \cdot \vec{x}}\right), & \text{if } \vec{x} \cdot \vec{y} < 0 \\ \text{sat}\left(\vec{y}, \frac{-\vec{x} \cdot \vec{y} + \sqrt{(\vec{x} \cdot \vec{y})^2 + r^2 - \vec{x} \cdot \vec{x}}}{\vec{y} \cdot \vec{y}}\right), & \text{if } \vec{x} \cdot \vec{y} \geq 0 \end{cases} \tag{42a}$$

$$\text{sat}(\vec{w}, p) = \begin{cases} \vec{w}, & \text{if } \|\vec{w}\| \leq p \\ \frac{p}{\|\vec{w}\|}\vec{w}, & \text{if } \|\vec{w}\| > p \end{cases} \tag{42b}$$

NUMERICAL SIMULATION

In this section, the performance and robustness of the proposed law will be verified through several numerical simulations. The common parameters used throughout simulations are summarized in Table. 2 and some of them are adopted from the work of Açıkmeşe.[5]

Table 1. Parameters Used for Numerical Simulations

Parameters	Description	Value	Unit
g	Local gravitational acceleration of Mars	3.7114	m/s^2
m_{wet}	Mass of lander including fuel	1905	kg
m_{dry}	Mass of lander excluding fuel	1405	kg
$T_{\max}$	Upper bound of thrust	13260	N
$T_{\min}$	Lower bound of thrust	4972	N
α	Fuel consumption rate	4.53×10^{-4}	kg/N
k	Tracking control gain	2.5	-
C_β	Ratio for reference trajectory acceleration	0.9	-
C_e	Velocity tracking error threshold	20	m/s
C_{col}	Collision avoidance logic trigger threshold	0.7	-

Performance Analysis Simulation

Three different scenarios are tested to cover a wide range of initial conditions. Each case represents 'Small Initial Deviation', 'Large Initial Deviation', and 'Overshoot Initial Speed', respectively. In addition, four different control laws including the method of this paper are compared for each scenario, and they are 'Gravity Turn Guidance (GT)', 'Polynomial Guidance (Poly)', 'Zero-Effort-Miss/Zero-Effort-Velocity Guidance(ZEM/ZEV)', and 'Offline Fuel Optimal Trajectory (Optimal)'.[11,12] Note that the fuel optimal solutions are obtained by GPOPS and 4 degrees glide slope angle constraint is imposed.[22] For a computational time point of view, all three feedback control laws (GT, Poly, ZEM/ZEV) take less than 0.1 milliseconds in a standard MATLAB environment, but the optimal trajectory takes about 1 minute to get an accurate solution.

Case 1: Small Initial Deviation

The initial states for the scenario are $\vec{r}_0^L = [500,\ -2000,\ 1500]^T$ m and $\vec{v}_0^L = [30,\ 100,\ -20]^T$ m/s. The three-dimensional trajectory, time histories of the velocity, position, and acceleration are given in Figure. 7. The initial condition of the scenario has moderate deviation so that all methods are able to make the lander land safely at the desired landing site. One can check that the trajectory of the GT method shows a steep concave-down shape at the last moment, and the thrust direction becomes opposite of the nadir direction. The amount of fuel usage for each method is 204 kg (GT), 231 kg (Poly), 208 kg (ZEM/ZEV), and 190 kg (Optimal), respectively.

Case 2: Large Initial Deviation

The initial states for the scenario are $\vec{r}_0^L = [5000,\ -2000,\ 1000]^T$ m and $\vec{v}_0^L = [30,\ 100,\ -20]^T$ m/s. The three-dimensional trajectory, time histories of the velocity, position, and acceleration are given in Figure. 8. The initial condition of the scenario has a large deviation compared to the previous case. The figure shows that the trajectory of polynomial guidance collides with the ground and that of the ZEM/ZEV method barely flies over the ground. One can check that the trajectory of the GT method shows a steep concave-down shape at the last moment as expected. The amount of fuel usage for each method is 345 kg (GT), N/A kg (Poly), 364 kg (ZEM/ZEV), and 325 kg (Optimal), respectively.

Case 3: Overshoot Initial Speed

The initial states for the scenario are $\vec{r}_0^L = [500,\ 2000,\ 1500]^T$ m and $\vec{v}_0^L = [0,\ 100,\ -75]^T$ m/s. The three-dimensional trajectory, time histories of the velocity, position, and acceleration are given in Figure. 9. The initial condition of the scenario has a large deviation compared to the previous case. The trajectory figure shows only the GT method and Optimal were able to land safely. Figure. 10 shows the side view of the three-dimensional trajectory and it is shown that both methods did not violate the glide slope constraint. The amount of fuel usage for each method is 379 kg (GT), N/A kg (Poly), N/A kg (ZEM/ZEV), and 361 kg (Optimal), respectively.

Robustness Analysis Simulation

The simulations with the same scenarios but considering external disturbances are conducted to verify the robustness of the proposed law. In this paper, a quadratic drag and constant bias force were taken into account, and the parameters for disturbances are shown in Table. 2.

The time histories of the velocity and acceleration for each scenario are given in Figure. 11 to Figure. 13. The proposed method was able to land the lander safely even if there exist big enough disturbances. Note that the other two methods, Polynomial guidance and ZEM/ZEV guidance, collide with the ground due to the control saturation raised by disturbances. The figures of acceleration history clearly show the presence of bias disturbance and the proposed method was able to compensate the disturbances without any control saturation.

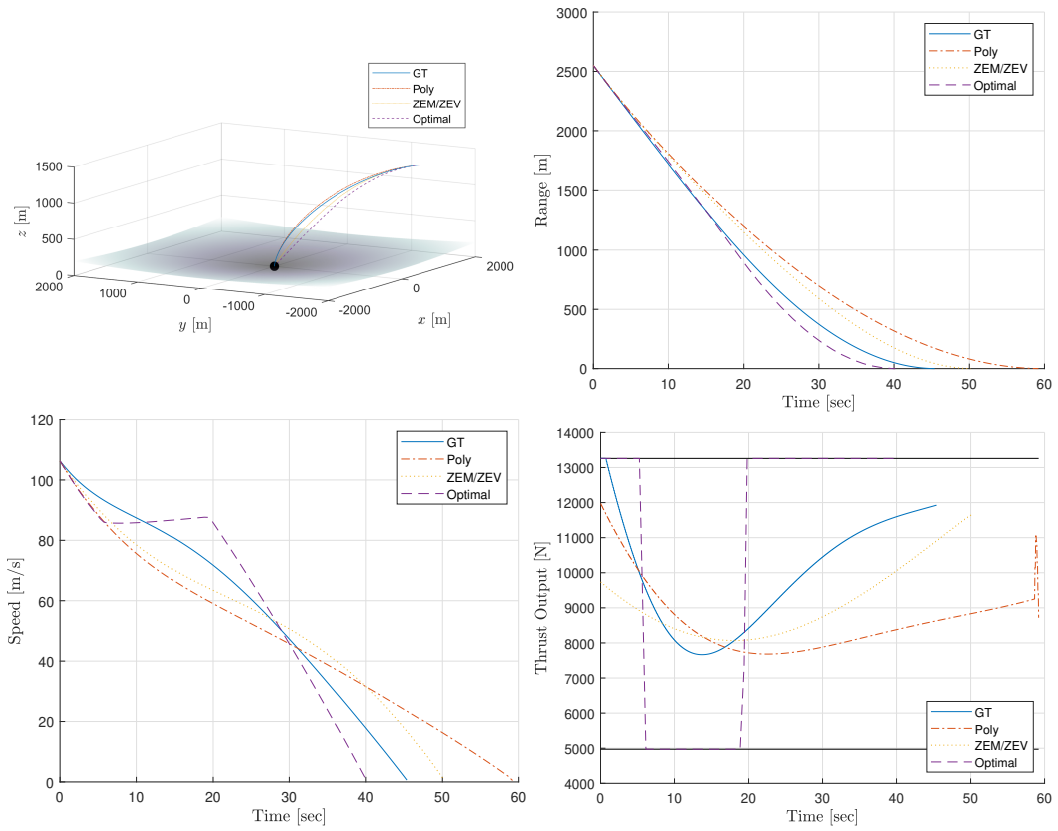

Figure 7. Simulation Results of Scenario 1 (a) Trajectory (b) Range (c) Speed (d) Control History

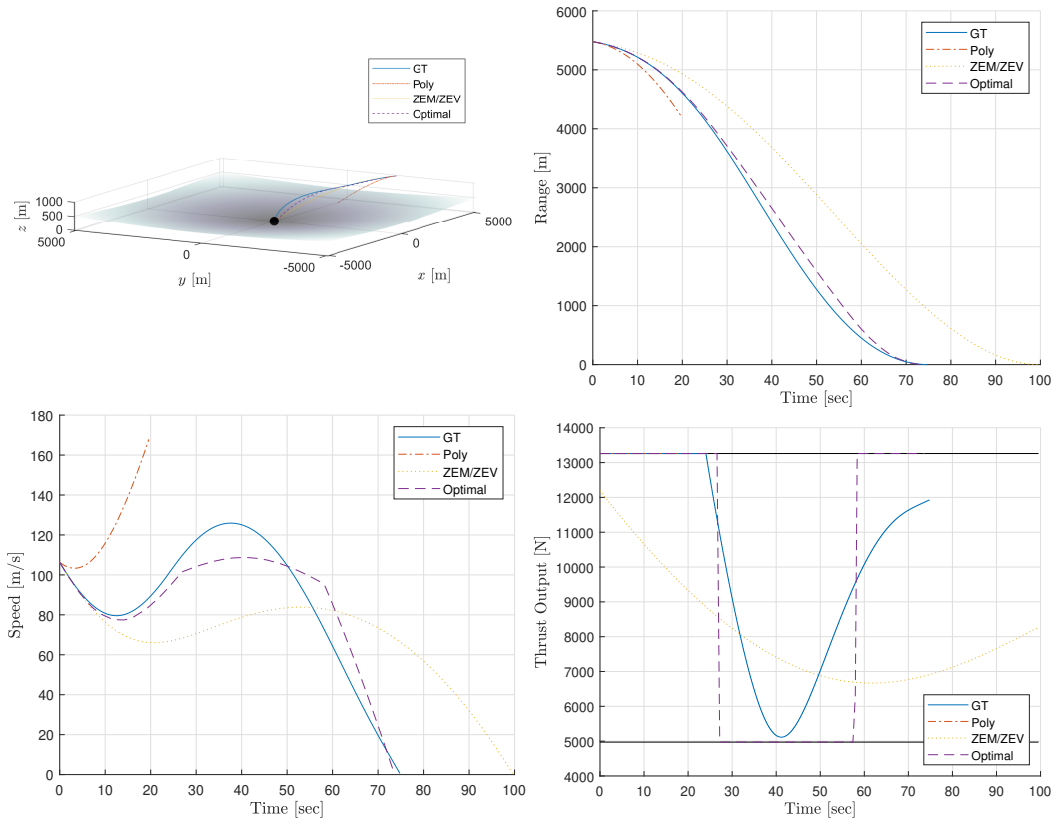

Figure 8. Simulation Results of Scenario 2 (a) Trajectory (b) Range (c) Speed (d) Control History

Table 2. Parameters of Disturbances Used for Robustness Analysis

Parameters	Description	Value	Unit
C_{drag}	Effective quadratic drag coefficient $(0.5\rho C_d S_{ref})$	0.0685	$\text{N} \cdot \text{s}^2/\text{m}^2$
b_x	Bias disturbance acceleration along x-axis	$0.25g$	-
b_y	Bias disturbance acceleration along y-axis	$0.25g$	-
b_z	Bias disturbance acceleration along z-axis	$-0.2g$	-

CONCLUSION

This work proposed a new method of velocity vector tracking law generated by the gravity turn trajectory for the terminal landing phase of a pinpoint landing mission. The paper investigated the appropriate properties of the gravity turn trajectory for a pinpoint landing mission and fully utilizes them to design guidance law. Thanks to the characteristics, the lander following the trajectory will avoid the ground obstacle and the final attitude will have zero pitch angle which is desirable. The nonlinear control law and intermediate ground collision avoidance logic were implemented to track the velocity vector safely and robustly within a finite time. Several representative scenarios were tested through a numerical simulation, and it turned out that the logic is capable of a pinpoint landing regardless of feasible initial conditions and the fuel consumption of the law is comparable to that of the optimal result considering the fact that the optimal trajectory has non-zero pitch angle at the last moment.

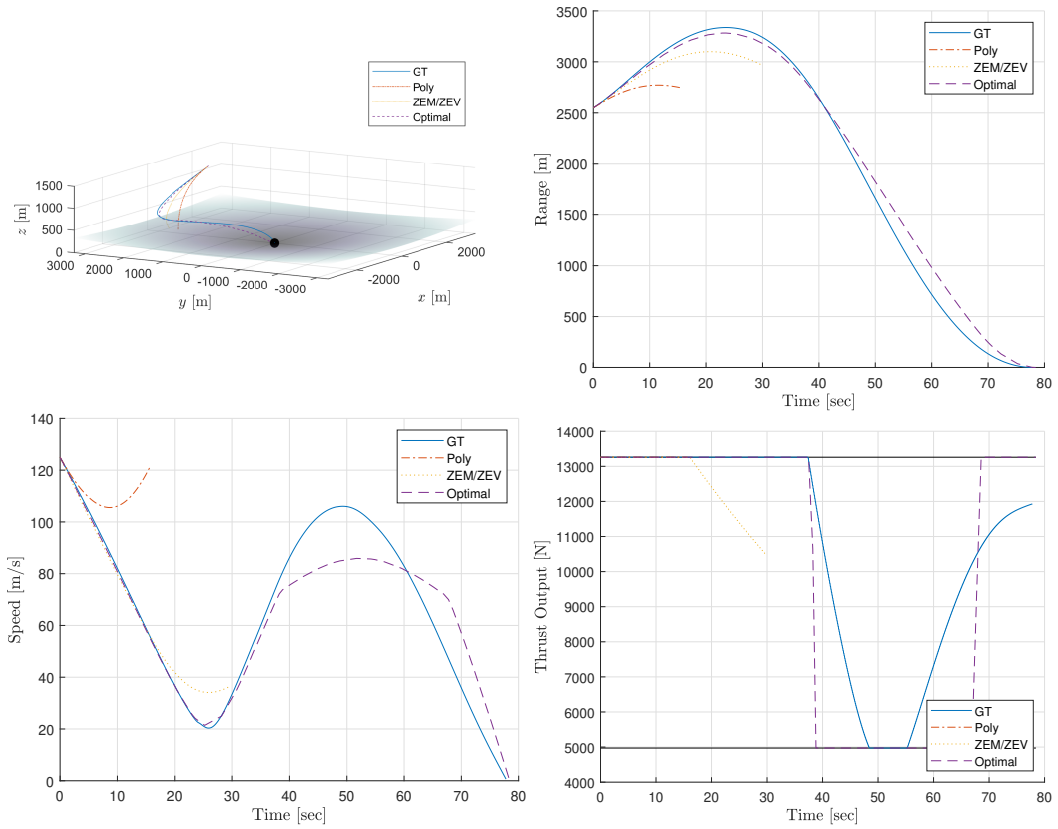

Figure 9. Simulation Results of Scenario 3 (a) Trajectory (b) Range (c) Speed (d) Control History

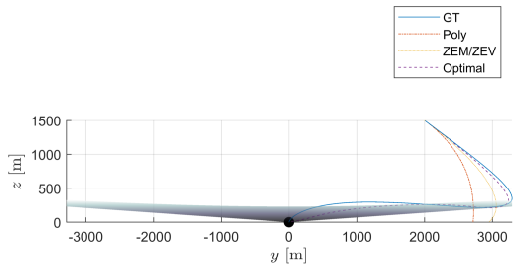

Figure 10. Side view trajectory of Scenario 3

Although the proposed method was analytically well-researched, several issues still remained including the proper way to select control gain and robustness against navigation error, and these topics will be covered in future work. In addition, the analytic solution of gravity turn trajectory under quadratic drag is available, so the method can be further improved by adopting the solution as covered in this paper.

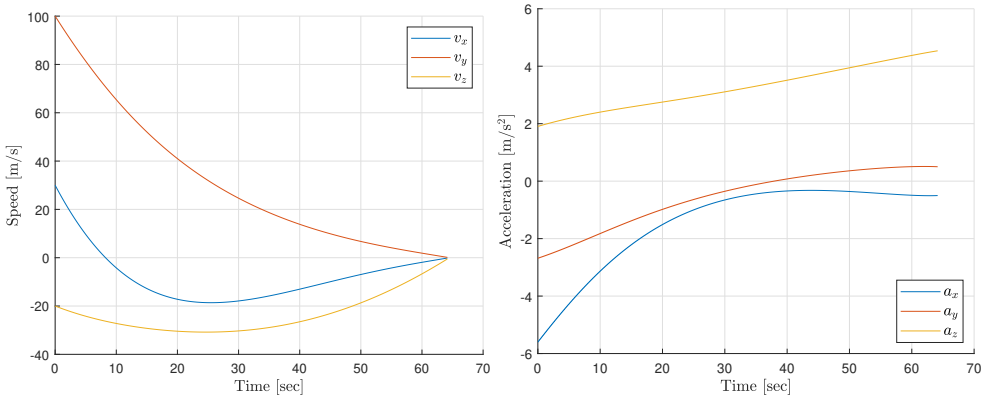

Figure 11. Simulation Results of Scenario 1 with Disturbances (a) Velocity (c) Acceleration Command History

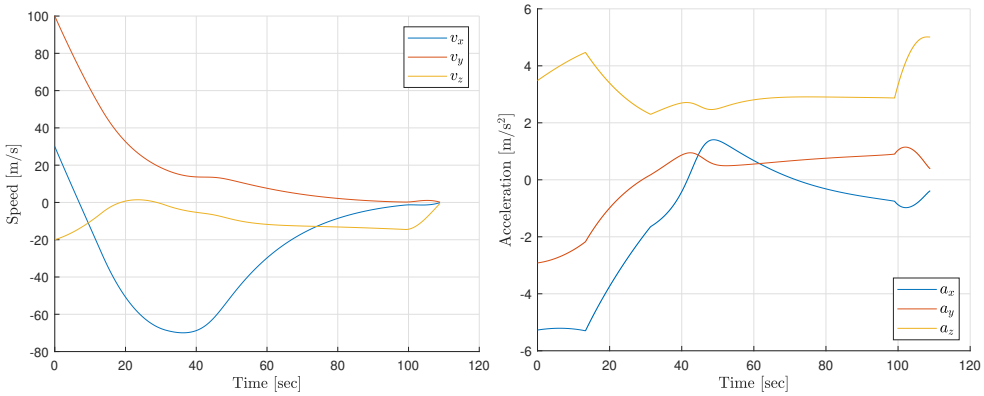

Figure 12. Simulation Results of Scenario 2 with Disturbances (a) Velocity (c) Acceleration Command History

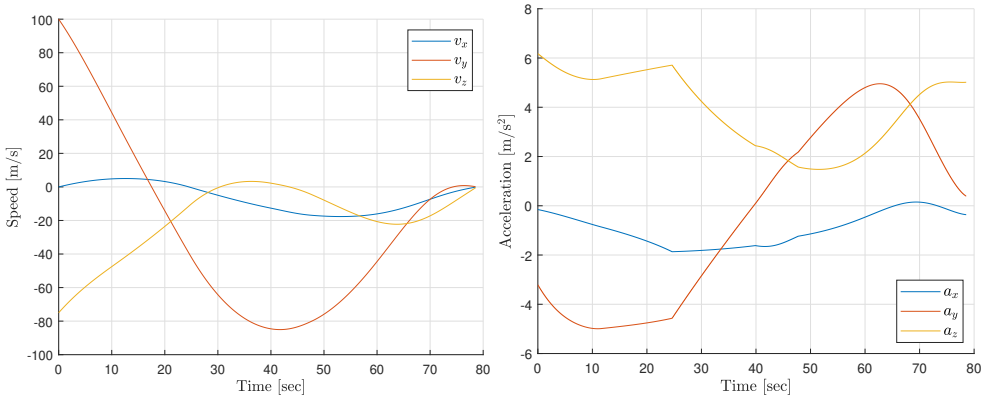

Figure 13. Simulation Results of Scenario 3 with Disturbances (a) Velocity (c) Acceleration Command History

REFERENCES

[1] NASA, "Artemis Plan - NASA's Lunar Exploration Program Overview," 2020.

[2] NASA, "NASA's Journey to Mars: Pioneering Next Steps in Space Exploration," 2015.

[3] R. R. Sostaric, C. J. Cerimele, E. A. Robertson, and J. A. Garcia, "A Rigid Mid Lift-to-Drag Ratio Approach to Human Mars Entry, Descent, and Landing," *AIAA Guidance, Navigation, and Control Conference*, 2017, p. 1898, 10.2514/6.2017-1898.

[4] M.-J. Tahk, S. Han, B.-Y. Lee, and J. Ahn, "Perch Landing Assisted by Thruster (PLAT): Concept and Trajectory Optimization," *International Journal of Aeronautical and Space Sciences*, Vol. 17, No. 3, 2016, pp. 378–390, 10.5139/IJASS.2016.17.3.378.

[5] B. Acikmese and S. R. Ploen, "Convex Programming Approach to Powered Descent Guidance for Mars Landing," *Journal of Guidance, Control, and Dynamics*, Vol. 30, No. 5, 2007, pp. 1353–1366, 10.2514/1.27553.

[6] D. Dueri, B. Açıkmeşe, D. P. Scharf, and M. W. Harris, "Customized Real-Time Interior-Point Methods for Onboard Powered-Descent Guidance," *Journal of Guidance, Control, and Dynamics*, Vol. 40, No. 2, 2017, pp. 197–212, 10.2514/1.G001480.

[7] P. Lu, "Propellant-Optimal Powered Descent Guidance," *Journal of Guidance, Control, and Dynamics*, Vol. 41, No. 4, 2018, pp. 813–826, 10.2514/1.G003243.

[8] A. R. Klumpp, "Apollo lunar descent guidance," *Automatica*, Vol. 10, No. 2, 1974, pp. 133–146, https://doi.org/10.1016/0005-1098(74)90019-3.

[9] R. Cheng, D. Conrad, and C. Meredith, "Design considerations for Surveyor guidance.," *Journal of Spacecraft and Rockets*, Vol. 3, No. 11, 1966, pp. 1569–1576.

[10] P. N. Desai, J. L. Prince, E. M. Queen, M. M. Schoenenberger, J. R. Cruz, and M. R. Grover, "Entry, Descent, and Landing Performance of the Mars Phoenix Lander," *Journal of Spacecraft and Rockets*, Vol. 48, No. 5, 2011, pp. 798–808, 10.2514/1.48239.

[11] Y. Guo, M. Hawkins, and B. Wie, "Applications of Generalized Zero-Effort-Miss/Zero-Effort-Velocity Feedback Guidance Algorithm," *Journal of Guidance, Control, and Dynamics*, Vol. 36, No. 3, 2013, pp. 810–820, 10.2514/1.58099.

[12] E. C. Wong, G. Singh, and J. P. Masciarelli, "Guidance and Control Design for Hazard Avoidance and Safe Landing on Mars," *Journal of Spacecraft and Rockets*, Vol. 43, No. 2, 2006, pp. 378–384, 10.2514/1.19220.

[13] Y. Guo, M. Hawkins, and B. Wie, "Waypoint-Optimized Zero-Effort-Miss/Zero-Effort-Velocity Feedback Guidance for Mars Landing," *Journal of Guidance, Control, and Dynamics*, Vol. 36, No. 3, 2013, pp. 799–809, 10.2514/1.58098.

[14] P. Cui, T. Qin, S. Zhu, Y. Liu, R. Xu, and Z. Yu, "Trajectory curvature guidance for Mars landings in hazardous terrains," *Automatica*, Vol. 93, 2018, pp. 161–171, https://doi.org/10.1016/j.automatica.2018.03.049.

[15] S. J. CITRON, S. E. DUNIN, and H. F. MEISSINGER, "A terminal guidance technique for lunar landing," *AIAA Journal*, Vol. 2, No. 3, 1964, pp. 503–509, 10.2514/3.2362.

[16] C. R. McInnes, "Direct Adaptive Control for Gravity-Turn Descent," *Journal of Guidance, Control, and Dynamics*, Vol. 22, No. 2, 1999, pp. 373–375, 10.2514/2.4392.

[17] C. T. Chomel and R. H. Bishop, "Analytical Lunar Descent Guidance Algorithm," *Journal of Guidance, Control, and Dynamics*, Vol. 32, No. 3, 2009, pp. 915–926, 10.2514/1.37700.

[18] S. Han, M.-C. Hwang, B.-Y. Lee, J. Ahn, and M.-J. Tahk, "Analytic Solution of Projectile Motion with Quadratic Drag and Unity Thrust," *IFAC-PapersOnLine*, Vol. 49, No. 17, 2016, pp. 40–45. 20th IFAC Symposium on Automatic Control in AerospaceACA 2016, https://doi.org/10.1016/j.ifacol.2016.09.008.

[19] S. Han, "Study on vertical landing of unmanned aerial vehicle using thrusters," Master's thesis, KAIST, 2017.

[20] S. Han, J. Ahn, and M.-J. Tahk, "Analytical Staring Attitude Control Command Generation Method for Earth Observation Satellites," *Journal of Guidance, Control, and Dynamics*, Vol. 45, No. 7, 2022, pp. 1347–1356, 10.2514/1.G006041.

[21] C.-H. Lee, H.-S. Shin, J.-I. Lee, and M.-J. Tahk, "Zero-Effort-Miss Shaping Guidance Laws," *IEEE Transactions on Aerospace and Electronic Systems*, Vol. 54, No. 2, 2018, pp. 693–705, 10.1109/TAES.2017.2764258.

[22] M. A. Patterson and A. V. Rao, "GPOPS-II: A MATLAB Software for Solving Multiple-Phase Optimal Control Problems Using Hp-Adaptive Gaussian Quadrature Collocation Methods and Sparse Nonlinear Programming," *ACM Trans. Math. Softw.*, Vol. 41, No. 1, 2014, 10.1145/2558904.